Comparison of Metal Artifact Reduction Algorithms in Patients with Hip Prostheses: Virtual Monoenergetic Images vs. Orthopedic Metal Artifact Reduction

고관절 인공치환술 환자에서 금속 인공물 감소 방법의 비교: 가상 단일에너지영상 대 금속 인공물 감소기법

Hye Jin Yoo, MD[1,2]* iD, Sung Hwan Hong, MD[1,2,3] iD,
Ja-Young Choi, MD[1,2] iD, Hee Dong Chae, MD[1,2] iD

[1]Department of Radiology, Seoul National University Hospital, Seoul, Korea
[2]Department of Radiology, Seoul National University College of Medicine, Seoul, Korea
[3]Institute of Radiation Medicine, Seoul National University Medical Research Center, Seoul, Korea

ORCID iDs
Hye Jin Yoo iD https://orcid.org/0000-0002-9704-7870
Sung Hwan Hong iD https://orcid.org/0000-0003-2302-1341
Ja-Young Choi iD https://orcid.org/0000-0002-3363-0629
Hee Dong Chae iD https://orcid.org/0000-0003-2624-1606

Purpose To assess the usefulness of various metal artifact reduction (MAR) methods in patients with hip prostheses.

Materials and Methods This retrospective study included 47 consecutive patients who underwent hip arthroplasty and dual-energy CT. Conventional polyenergetic image (CI), orthopedic-MAR (O-MAR), and virtual monoenergetic image (VMI, 50–200 keV) were tested for MAR. Quantitative analysis was performed in seven regions around the prostheses. Qualitative assessments included evaluation of the degree of artifacts and the presence of secondary artifacts.

Results The lowest amount of image noise was observed in the O-MAR, followed by the VMI. O-MAR also showed the lowest artifact index, followed by high-keV VMI in the range of 120–200 keV (soft tissue) or 200 keV (bone). O-MAR had the highest contrast-to-noise ratio (CNR) in regions with severe hypodense artifacts, while VMI had the highest CNR in other regions, including the periprosthetic bone. On assessment of the CI of pelvic soft tissues, VMI showed a higher structural similarity than O-MAR. Upon qualitative analysis, metal artifacts were significantly reduced in O-MAR, followed by that in VMI, while secondary artifacts were the most frequently found in the O-MAR ($p < 0.001$).

Conclusion O-MAR is the best technique for severe MAR, but it can generate secondary artifacts. VMI at high keV can be advantageous for evaluating periprosthetic bone.

Index terms Artifacts; Prosthetic Implants; Metals; Multidetector Computed Tomography; Dual Energy Scanned Projection Radiography

INTRODUCTION

Metal artifacts can be produced by beam hardening, scatter, noise, photon starvation and edge effects (1, 2). These contributors result in corrupted data for the reconstruction of near metal tissue, ultimately causing an unreliable representation of the tissue. Thus, artifacts caused by metal implants hinder the diagnostic accuracy of CT images in the visualization of bone, bone-metal interfaces and soft tissue structures (1). Among the current metal artifact reduction (MAR) approaches, iterative reconstruction (IR) algorithms have been used to minimize scatter and edge effects (1, 3). However, the use of IR techniques is computationally intensive and possibly reduces spatial resolution. MAR algorithms identify the corrupted projection data caused by the presence of metal and subsequently replace this corrupted projection data with interpolated data of neighboring detector elements (1, 4, 5). The MAR technique appears particularly useful in the presence of large amounts of metal with low radiation doses, but it can generate secondary artifacts, especially in light metal alloy (titanium) (1, 6). Virtual monoenergetic images (VMIs) are acquired with two photon spectra at different energy levels using dual-energy CT. VMI acquired at high energies reduce beam-hardening artifacts by minimizing the influence of low-energy photons (1). However, acquiring VMI is not feasible with older generation CT scanners, and the use of VMI alone appears to be insufficient in the presence of heavy metals, such as stainless steel and cobalt chromium alloys (1, 7, 8).

To date, few side-by-side comparisons of their diagnostic performance in the reduction of metal artifacts have been conducted. Hence, the purpose of this study was assess the effects of MAR and VMI and to evaluate the secondary artifacts generated by MAR methods in patients with hip prostheses.

MATERIAL AND METHODS

PATIENTS

The study was approved by our Institutional Review Board, and written informed consent was waived due to the retrospective nature of the study (IRB No. 1812-007-991). Between April 2017 and July 2018, 47 consecutive patients who underwent hip arthroplasties (bilateral, 11; unilateral, 36) were included in this study. There were 28 male and 19 female, and the mean age was 63.2 $\pm$ 10.7 years old. The reason of CT examination was routine follow-up after hip surgery ($n = 24$) or hip pain ($n = 23$).

CT EXAMINATION

All CT scans were performed using a first-generation dual-layer spectral detector CT scanner (IQon Spectral CT; Philips Healthcare, Best, the Netherland). The following scanning parameters were used: tube voltages of 120 kVp; a slice acquisition of 64 × 0.625 mm collimation; a rotation time of 0.64 seconds; a beam pitch of 0.67; a field of view of 400 × 400 mm; a volume CT dose index of 10–11 mGy; and a dose length product of 300–366 mGy*cm.

IMAGE RECONSTRUCTION

Conventional polyenergetic images (CIs) were reconstructed using an IR algorithm (iDose Level 2, Philips Healthcare, Cleveland, OH, USA) at 120 kVp, which is used in clinical practice. MAR images were reconstructed from CI with an orthopedic MAR algorithm (O-MAR, Philips Healthcare). VMI were generated from spectral raw data using a dedicated workstation (Intellispace Portal, Philips, Best, the Netherland) at settings ranging from 50 keV to 200 keV in increments of 10 keV. Then, the VMI were transferred to the PACS system workstations (IN-FINITT; Infinitt Healthcare, Seoul, Korea) for the imaging analysis of the monoenergetic CT images. All images were reconstructed at a 2 mm slice thickness with 1 mm of overlap and a YD filter.

QUANTITATIVE ASSESSMENT

Assessments of three kind of image sets were separately performed by a radiologist with 5 years of experience in musculoskeletal imaging, and then reviewed by the other musculoskeletal radiologist with 10 years of experience. For the quantitative assessment, the following regions of interest (ROIs) were drawn as large as possible in CIs in the bone window (width 2000 Hounsfield unit [HU], center 500 HU) on a representative axial plane at the level of the artificial femoral head, where the metal artifact was the strongest: a) anterior acetabulum, b) posterior acetabulum, c) anterior psoas muscle, d) medial pelvic wall, e) lateral hip, f) posterior gluteus muscle, and g) air outside of the metal artifact (Fig. 1). The medial pelvic wall (d) and lateral hip (e) were the areas with the most pronounced hypodense artifacts. If metal prostheses were present in both hips, the right prosthesis of the patient was evaluated. The ROIs were then transferred to the O-MAR images and VMI, while the size and location of the ROIs were

Fig. 1. Regions of interest are placed in seven areas, including the (a) anterior acetabulum, (b) posterior acetabulum, (c) anterior psoas muscle, (d) medial pelvic wall, (e) lateral hip, (f) posterior gluteus muscle, and (g) air outside the metal artifact.

maintained. In all ROIs, the CT number (HU) and standard deviation (SD) were recorded. To correct for less image noise in the high-keV images compared to the low-energy VMI and CI, image noise within the air outside of the metal artifact was subtracted from the respective SD, yielding the corrected image noise ($cIN_x = SD_x – SD_{air}$) (9). The artifact index (AI) was introduced to quantify the severity of the metal artifacts ($AI = SQRT [SD_x^2 – SD_{air}^2]$), where SD_x represents the SD in the artifacts and SD_{air} represents the SD in the air (10, 11). The contrast-to-noise ratio (CNR) was calculated as follows: CNR = (mean CT number [ROI x] – mean CT number [ROI air])/ SD air) (12). Additionally, the structural similarity (SSIM) was used to quantitatively evaluate the performance of metal artifact correction (13, 14). The SSIM index was computed using open source software (http://icy.bioimageanalysis.org/download) for the ROIs A and B for each patient (Fig. 2). ROI A surrounded the metallic object and was used to evaluate the similarity of the corrected image (O-MAR and VMI) to the original metallic structure on uncorrected images (CI). ROI B was positioned between the femoral heads and was used to evaluate the similarity hampered by the streak and shadow artifacts. We used the CI as reference images to compute the SSIM.

QUALITATIVE ASSESSMENT

Qualitative assessments of three kind of image sets were separately performed by two radiologists with 10 and 5 years of experience in musculoskeletal imaging. The degree of the metal artifacts was graded on a four-point rating scale (0 = denoted no metal artifacts, 1 = mild metal artifacts without impairment of adjacent structural depiction, 2 = moderate metal artifacts with considerable impairment but considered diagnostic, 3 = severe artifacts and considered nondiagnostic). Additionally, several secondary artifacts on O-MAR images were evaluated, which were previously reported as newly developed artifacts on O-MAR images (6, 15). The conspicuity of intramedullary bone trabeculae was rated using a 4-point scale (0 = recognition with high confidence, 1 = recognition with medium confidence, 2 = faint demarcation with low confidence, 3 = nearly absent and questionable). The degrees of artifactual cortical thinning or perforation and pseudocemented appearance were also rated using a 4-point scale (0 = nearly absent, 1 = present with low confidence, 2 = present with medium confidence, 3 = present with high confidence). The ratings were performed in the axial plane with a typical bone window setting (width, 2000 HU; center, 500 HU). The scores from two ob-
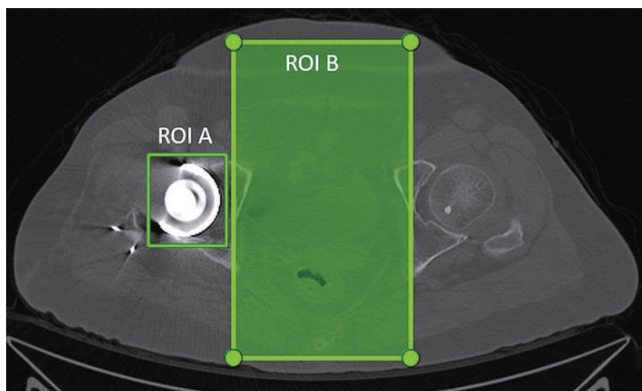
Fig. 2. The SSIM index is computed in ROIs A and B for each patient. ROI A surrounds the metallic object; it is used to evaluate the similarity of the corrected image (orthopedic-metal artifact reduction and virtual monoenergetic image) relative to the original metallic structure on uncorrected images (CI). ROI B is positioned between the femoral heads and is used to evaluate the similarity hampered by the streak and shadow artifacts. The CI is used as reference to compute the SSIM.
CI = conventional image, ROI = regions of interest, SSIM = structural similarity

servers were averaged for statistical analysis.

STATISTICAL ANALYSIS

For statistical analyses, SPSS (version 22; IBM Corp., Armonk, NY, USA) and MedCalc Software (version 16.2.1; MedCalc Software, Ostend, Belgium) were used. Continuous variables were expressed as the means $\pm$ SD. A two-tailed p value < 0.05 was considered statistically significant. The quantitative and qualitative assessments were also compared among the three methods using repeated-measures Friedman rank-sum test and subsequently pairwise comparisons were carried out using the Wilcoxon signed-rank test.

RESULTS

QUANTITATIVE ASSESSMENT

Table 1 and Fig. 3 show summaries of the quantitative assessment. There was no significant difference of CT number, SD, and AI between patients with unilateral or bilateral prosthesis. In terms of CNR, patients with unilateral prosthesis showed higher CNR compared to patients with bilateral prosthesis.

Table 1. Mean Values of Quantitative Assessment

Location	Methods	Mean of HU	SD of HU	cIN (Reduction %)*	AI (Reduction %)	CNR (Increment %)
Aceta_A	CI	147.25	235.86	185.49	233.24	37.58
	O-MAR	60.88	130.70	93.23 (49.7)	127.52 (45.3)	44.59 (18.6)
	VMI	152.87	153.34	109.34 (41.0)	151.84 (34.9)	59.75 (59.0)
Aceta_P	CI	341.00	200.88	150.50	197.94	43.69
	O-MAR	144.63	132.95	95.47 (36.6)	129.77 (34.4)	48.16 (10.2)
	VMI	195.18	139.48	95.49 (36.6)	137.84 (30.4)	61.60 (41.0)
Ant	CI	189.23	113.28	62.90	108.30	38.96
	O-MAR	97.46	65.01	27.53 (56.2)	59.69 (44.9)	45.94 (17.9)
	VMI	162.88	87.27	44.82 (31.2)	86.25 (21.7)	59.31 (52.2)
Med	CI	-427.80	110.33	59.96	105.26	19.11
	O-MAR	-142.38	65.40	27.92 (53.4)	60.14 (42.9)	36.09 (88.8)
	VMI	-379.14	95.80	51.68 (14.0)	93.25 (11.5)	33.85 (77.1)
Lat	CI	-362.11	149.85	99.47	145.52	21.12
	O-MAR	-37.44	61.57	24.09 (75.8)	55.60 (61.8)	40.39 (91.2)
	VMI	-386.75	118.86	76.91 (24.7)	118.70 (19.8)	31.85 (50.8)
Glu_ip	CI	66.43	80.25	29.88	73.44	35.14
	O-MAR	62.99	52.87	15.39 (48.5)	46.25 (37.0)	44.46 (26.5)
	VMI	62.10	66.79	23.24 (23.7)	63.81 (13.4)	54.62 (55.4)

*Data in the parentheses indicate reduction or increment of each variable in MAR techniques compared to CI.
Aceta_A = anterior acetabulum, Aceta_P = posterior acetabulum, AI = artifact index, Ant = anterior psoas muscle, CI = conventional image, cIN = corrected image noise, CNR = contrast-to-noise ratio, Glu-ip = posterior gluteus muscle, HU = Hounsfield unit, Lat = lateral hip, Med = medial pelvic wall, O-MAR = orthopedic-metal artifact reduction, SD = standard deviation, VMI = virtual monoenergetic image

Fig. 3. Quantitative assessment using average CT number (A), image noise (B), AI (C) and CNR (D) of all representative regions.
A. Average CT number shows a marked increase in the O-MAR images when severe hypodense artifacts are present (medial and lateral regions). However, the CT number in other regions is significantly lower in the O-MAR images. High-keV (≥ 80 keV) VMI also shows HU values similar (anterior acetabulum) or lower than those of the CI.
B. The lowest cIN is found in the O-MAR images in all regions, followed by that in the VMI.
C. The AI is the lowest in the O-MAR images, followed by that in the high-keV VMI, in all regions except the posterior acetabulum, wherein the O-MAR images and the 200-keV VMI showed comparable AIs. In the VMI, the AI decreases with increasing keV, with the lowest value at 200 keV in all the regions except the medial pelvic wall, where the lowest AI corresponds to 130 keV.
D. The VMI shows a tendency toward an increasing CNR with increasing keV. The VMI shows the highest CNR in all regions, except the medial and lateral regions; the O-MAR images show the highest CNR in the medial and lateral regions.
AI = artifact index, CI = conventional image, cIN = corrected image noise, CNR = contrast-to-noise ratio, HU = Hounsfield unit, O-MAR = orthopedic-metal artifact reduction, VMI = virtual monoenergetic image
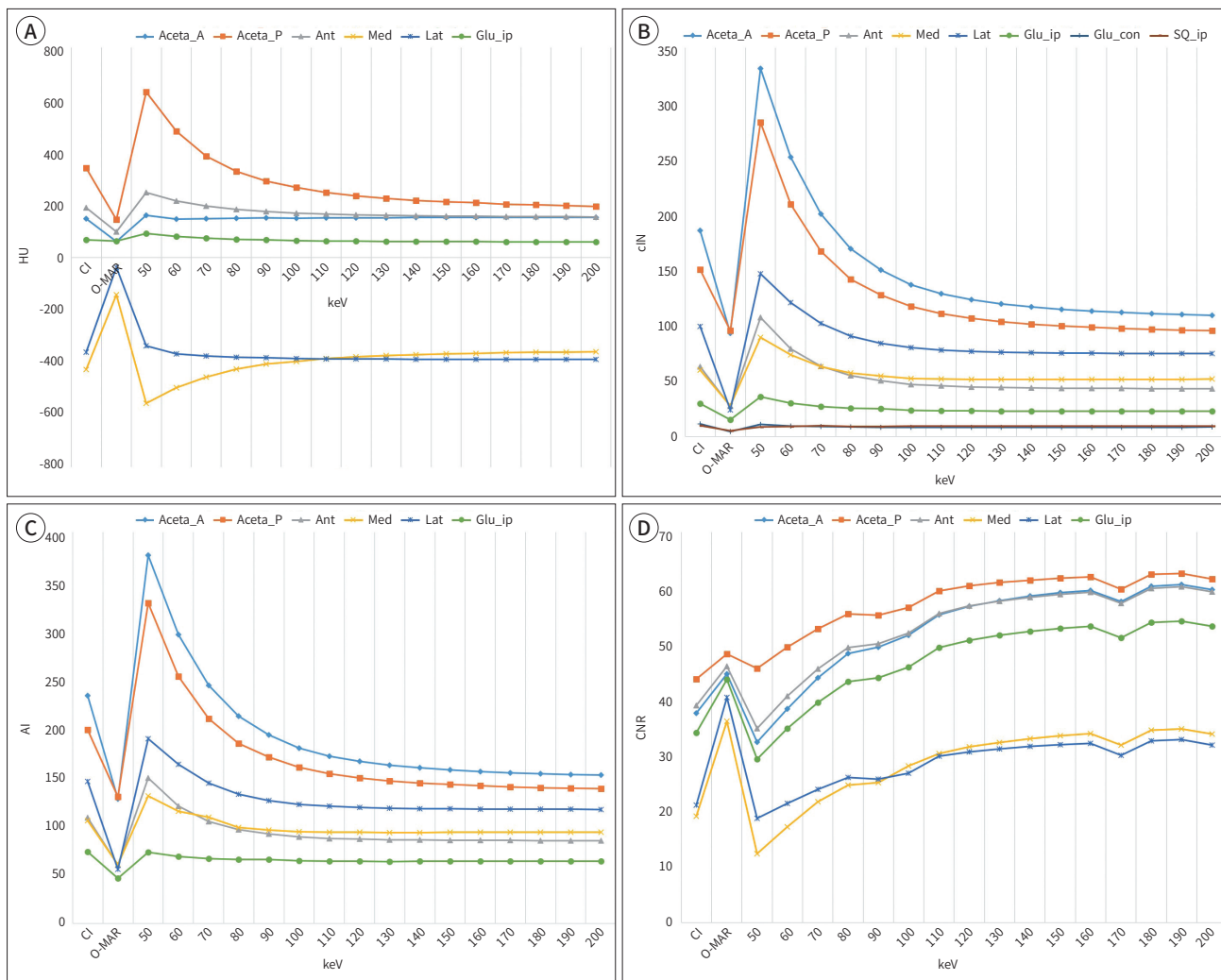
AVERAGE CT NUMBER

Attenuation within the medial and lateral regions, where severe hypodense artifacts were present, markedly increased in the O-MAR images because hypodense artifacts were erased in the O-MAR images. In those two regions, the O-MAR images showed significantly higher HU values than did the CI and VMI ($p < 0.001$), but the VMI showed similar (lateral) or slightly higher (medial) HU values than did the CI (Fig. 3). However, in other regions without hy-

podense artifacts, the CT number was significantly lower in the O-MAR images compared to the CI. In the regions without hypodense artifacts, the VMI showed a decreasing tendency of attenuation as increasing keV on VMI. Thus, VMI of 80 keV or greater also showed HU values that were similar (anterior acetabulum) or lower than those of the CI. Within the posterior gluteus muscle (which was visually not affected by artifacts), the CI exhibited no difference in attenuation compared with other MAR images ($p > 0.05$).

CIN

The least amount of cIN was found in the O-MAR images in all regions, followed by the VMI (Fig. 3). The O-MAR images showed significant noise reduction compared to the VMI, except for the 200 keV VMI, which showed comparable image noise in acetabular bone ($p > 0.1$). In all regions, the amount of cIN was significantly lower in the O-MAR images than in the CI ($p < 0.001$), ranging from 36.6% (posterior acetabulum) to 75.8% (lateral hip) noise reduction. The VMI of 80 keV or greater also showed significant noise reduction compared to the CI ($p < 0.05$), ranging from 13.8% (medial pelvic wall) to 41.1% (anterior acetabulum) noise reduction.

AI

The AI was found to be the lowest in the O-MAR images ($p < 0.001$), followed by the high-keV VMI, in all regions except the posterior acetabulum, where the O-MAR images and 200 keV VMI showed comparable AIs ($p = 0.057$) (Fig. 3). In the VMI, the AI decreased with increasing keV and was the lowest at 200 keV in all regions except the medial pelvic wall, where the lowest AI was found at 130 keV. However, there was no significant difference in the AI in the range of 120–200 keV in soft tissue regions. In acetabular bone, the AI at 200 keV was significantly lower than those at other monoenergy levels ($p < 0.001$).

CNR

The VMI showed a tendency towards an increasing CNR with increasing keV. Among the three image settings, CNR was found to be highest in the VMI in all regions except the medial and lateral regions, where the hypodense artifacts are the most severe (Fig. 3). The increase in CNR ranged from 41.0% (posterior acetabulum) to 59.0% (anterior acetabulum) in the 200 keV VMI compared to the CI. In the medial and lateral regions with severe hypodense artifacts, the O-MAR images showed a higher CNR ($p < 0.001$), with an increase in CNR ranging from 88.8% (medial) to 91.2% (lateral), compared to the CI.

Table 2. Structural Similarity Index Values

	ROI A*		ROI B[†]	
	CI vs. O-MAR	CI vs. VMI (200 keV)	CI vs. O-MAR	CI vs. VMI (200 keV)
Mean (range)	0.713 (0.132–0.918)	0.719 (0.459–0.856)	0.856 (0.046–0.962)	0.933 (0.554–0.964)

*ROI A surrounds the metallic object.
[†] ROI B is positioned in between the femoral heads.
CI = conventional image, O-MAR = orthopedic-metal artifact reduction, ROI = regions of interest, VMI = virtual monoenergetic image

Table 3. Qualitative Assessment

Methods	Degree of Metallic Artifact*		Conspicuity of Intramedullary Trabeculae[†]		Cortical Thinning or Perforation[‡]		Pseudocemented Appearance[‡]	
	Mean	SD	Mean	SD	Mean	SD	Mean	SD
CI	2.82 (2–3)	0.387	0.35 (0–3)	0.772	0.07 (0–3)	0.446	0.01 (0–3)	0.103
O-MAR	1.04 (0–2)	0.250	2.01 (0–3)	0.945	2.01 (0–3)	1.021	1.16 (0–1)	1.120
VMI	2.56 (0–3)	0.712	0.84 (0–3)	0.833	0.80 (0–3)	0.770	0.01 (0–1)	0.103

*0 = denoted no metal artifact, 1 = mild metal artifacts without impairment of adjacent structural depiction, 2 = moderate metal artifacts with considerable impairment but diagnostic, 3 = severe artifact and nondiagnostic.
[†]0 = denoted recognition with high confidence, 1 = recognition with medium confidence, 2 = faint demarcation with low confidence, 3 = nearly absence and questionable.
[‡]0 = nearly absence, 1 = presence with low confidence, 2 = presence with medium confidence, 3 = presence with high confidence.
CI = conventional image, O-MAR = orthopedic-metal artifact reduction, SD = standard deviation, VMI = virtual monoenergetic image

Fig. 4. A 70-year-old female who underwent right total hip arthroplasty.
A. Postoperative conventional images reconstructed using the iterative reconstruction algorithm (iDose level 2) show marked hypodense artifacts in the medial pelvic wall and lateral hip regions.
B. Postoperative CT scans reconstructed with 200-keV virtual monoenergetic images are less effective in metal artifact reduction.
C. Postoperative CT scans reconstructed with the orthopedic metal artifact reduction algorithm are the most optimal for hypodense metal artifact reduction (thin arrows), but the bone cortex seems to be thin or focally perforated (thick arrow) in these images.

SSIM

Table 2 summarizes the similarity measures at ROIs A and B, which are shown in Fig. 2. In ROI A, the VMI showed a similar SSIM value to that of the O-MAR images ($p = 0.333$). However, the SSIM value of the VMI in ROI B was significantly higher than that of the O-MAR images ($p < 0.001$), which indicates that the artifacts in the VMI were more similar to those in the CI than to those in the O-MAR images.

QUALITATIVE ANALYSIS

Table 3 shows summaries of the qualitative assessment. The degree of metal artifacts was significantly reduced in the O-MAR images, followed by the VMI and CI ($p < 0.001$). The conspicuity of intramedullary trabeculae was reported to be the best on the CI, followed by the VMI and O-MAR images ($p < 0.001$) (Table 3). Cortical thinning or focal perforation was frequently observed on the O-MAR images (35 [observer 1] and 31 [observer 2] patients) (Figs. 4, 5). Intramedullary trabeculae were obscured in 34 (observer 1) and 31 (observer 2) patients on the O-MAR images and 9 (observer 1) and 7 (observer 2) patients on the VMI (Fig. 5). No one showed these artifactual cortical changes in the CI. Pseudocemented appearance was reported on only the O-MAR images (22 [observer 1] and 19 [observer 2] patients) (Fig. 5). There

Fig. 5. A 54-year-old male who underwent right total hip arthroplasty.
A. Postoperative conventional images reconstructed using an iterative reconstruction algorithm (iDose level 2) show fine bone trabeculae and intact cortical lining in the acetabular bone.
B. Postoperative CT scans reconstructed with 200-keV virtual monoenergetic images show reduced hypodense metal artifacts, while also demonstrating a decreased CT number and partly blurred cortex in the acetabular bone (arrows).
C. Postoperative CT scans reconstructed with O-MAR algorithm show fine acetabular bone trabeculae that are barely delineated; moreover, the bone cortex seemed to have disappeared (thick arrows). The O-MAR image also shows a smudged high-attenuation area (thin arrow) around the acetabular implant.
O-MAR = orthopedic-metal artifact reduction
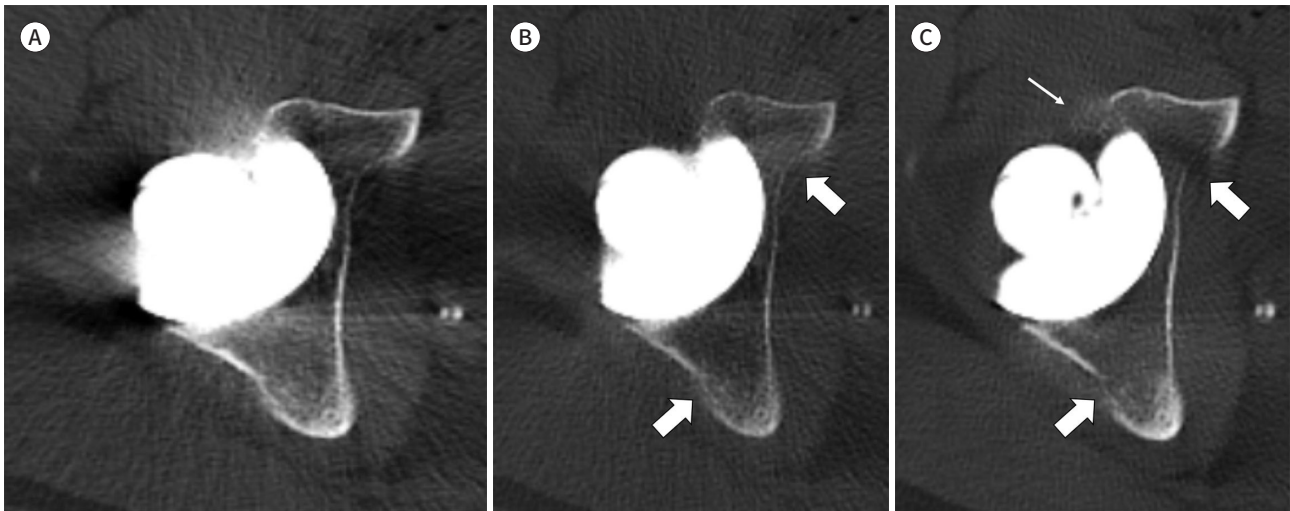
was no significant difference between the CI and VMI in the presence of pseudocemented appearance (*p* = 1.00).

DISCUSSION

In our study, O-MAR was effective for MAR because it showed the least amount of image noise and was associated with the lowest AI in patients with hip prostheses. In the subjective assessment, metal artifact was also significantly reduced with O-MAR. However, the O-MAR images showed lower CNRs than the high-keV VMI in most of the investigated regions, except in regions with severe hypodense streak artifacts. Additionally, the O-MAR images most frequently generated secondary artifacts (6).

There were two previous studies that directly compared CI, VMI and O-MAR images in MAR, which are similar to our study (9, 16). Große Hokamp et al. (9) showed that artifacts depicted by noise were reduced in both O-MAR images and high-keV VMI compared to CI, and subjectively, both methods yielded artifact reduction in most cases. Laukamp et al. (16) also demonstrated that both methods can reduce metal artifacts, but VMI was more effective in reducing moderately strong artifacts, while O-MAR was superior to other method in the reduction of strong artifacts. Previously, Wellenberg et al. (8) also stated that VMI are quite useful in reducing beam hardening artifacts caused by the absorption of low energy photons rather than severe artifacts caused by extensive photon starvation (8). Laukamp et al. (16) also demonstrated that O-MAR images proved to be advantageous for a pelvic soft tissue analysis. Similarly, our results demonstrated that O-MAR images are better than VMI in the

evaluation of pelvic soft tissue between the femoral heads by SSIM index analysis. They also found that VMI were especially helpful for the assessment of the metal-bone interfaces and for the reduction of hyperdense artifacts, while the iterative MAR method improved the evaluation of soft tissue and reduced hypodense artifacts (16). Our study also showed that VMI were helpful for assessing periprosthetic bone by reducing image noise and improving CNR in the periprosthetic bone. Furthermore, the VMI were not hampered by new artifacts and image distortion, while the MAR images yielded at least moderate image distortion, blurring and bone deletion (1, 6, 16, 17). Shim et al. (6) showed that O-MAR images tended to generate new artifacts including a pseudocemented appearance and scapular pseudonotching. Laukamp et al. (16) also reported that O-MAR led to additional streak artifacts and distinct image distortion, which were not observed in VMI. In accordance with these studies, we found that intramedullary trabeculae near the implant were less conspicuous or sometimes obscured due to the smoothing effect of O-MAR, and moreover, the cortex seemed to be thin or focally perforated in more than half of the patients. As reported by Shim et al. (6), a pseudocemented appearance was more frequently observed on the O-MAR images. Secondary artifacts introduced by the O-MAR algorithms might lead to a misdiagnosis of periprosthetic osteolysis; thus, O-MAR images should be used as supplementary images to conventional CT images and not as a replacement.

There was no generalized optimal energy level of VMI to reduce metal artifacts because the optimal level might depend on the metal alloy, shape and geometry of the implant. Wellenberg et al. (8) suggested an optimal monoenergetic energy of 130 keV for hip prostheses, and Meinel et al. (18) found that the optimal median energy level was 113 keV in patients with titanium and steel hip prostheses. Neuhaus et al. (19) found that in general, 140 keV was optimal, while 200 keV was selected as the optimal level for all cases. In our study, the lowest AI was found in the range of 120–200 keV in soft tissue regions and at 200 keV in periprosthetic bones. Additionally, we found that CNRs increased with increasing keVs on the VMI. Therefore, we suggested that 200 keV was the optimal keV for the evaluation of both periprosthetic soft tissues and bones to maintain relatively high CNRs.

There were several limitations in our study. First, our study was a retrospective study and included a relatively small sample size. Second, the participants underwent different types of surgeries, including unilateral and bilateral total hip arthroplasties and bipolar hemiarthroplasty. Third, we conducted attenuation, noise, AI, and CNR measurements to illustrate the extent of metal artifacts. However, it needs to be discussed which objective parameters are the best parameters for the evaluation of the metal artifacts. Fourth, bone resorption or osteolysis around prosthesis could affect CT number measurement, which could be a limitation in the periprosthetic bone evaluation. Finally, our study included only a small number of patients with periprosthetic complications, which are important problems in patients with hip prostheses but may be obscured by artifacts arising from metallic prostheses. Thus, whether MAR techniques can improve diagnostic accuracy in detecting these complications or alter the clinical decision cannot be tested. Therefore, additional clinical studies are necessary to show the difference among MAR techniques in evaluating periprosthetic complications.

In conclusion, O-MAR is the best technique for severe MAR caused by hip prostheses and for maintaining soft tissue contrast in periprosthetic soft tissues, even though it can generate

new secondary artifacts. VMI at high keV are less effective for severe MAR, but they can have advantages for the evaluation of periprosthetic bone.

Author Contributions

Conceptualization, Y.H.J., H.S.H., C.J.; data curation, Y.H.J.; formal analysis, Y.H.J., C.H.D.; funding acquisition, Y.H.J., H.S.H.; investigation, Y.H.J., C.H.D.; methodology, all authors; project administration, Y.H.J., H.S.H.; resources, all authors; software, Y.H.J., C.H.D.; supervision, H.S.H., C.J.; validation, H.S.H., C.J., C.H.D.; visualization, Y.H.J.; writing—original draft, Y.H.J., H.S.H.; and writing—review & editing, H.S.H., C.J., C.H.D.

Conflicts of Interest

The authors have no potential conflicts of interest to disclose.

Funding

REFERENCES

1. Wellenberg RHH, Hakvoort ET, Slump CH, Boomsma MF, Maas M, Streekstra GJ. Metal artifact reduction techniques in musculoskeletal CT-imaging. *Eur J Radiol* 2018;107:60-69
2. Boas FE, Fleischmann D. CT artifacts: causes and reduction techniques. *Imaging Med* 2012;4:229-240
3. Mallinson PI, Coupal TM, McLaughlin PD, Nicolaou S, Munk PL, Ouellette HA. Dual-energy CT for the musculoskeletal system. *Radiology* 2016;281:690-707
4. Kalender WA, Hebel R, Ebersberger J. Reduction of CT artifacts caused by metallic implants. *Radiology* 1987;164:576-577
5. Lell MM, Wildberger JE, Alkadhi H, Damilakis J, Kachelriess M. Evolution in computed tomography: the battle for speed and dose. *Invest Radiol* 2015;50:629-644
6. Shim E, Kang Y, Ahn JM, Lee E, Lee JW, Oh JH, et al. Metal artifact reduction for orthopedic implants (O-MAR): usefulness in CT evaluation of reverse total shoulder arthroplasty. *AJR Am J Roentgenol* 2017;209:860-866
7. Huang JY, Kerns JR, Nute JL, Liu X, Balter PA, Stingo FC, et al. An evaluation of three commercially available metal artifact reduction methods for CT imaging. *Phys Med Biol* 2015;60:1047-1067
8. Wellenberg RH, Boomsma MF, van Osch JA, Vlassenbroek A, Milles J, Edens MA, et al. Quantifying metal artefact reduction using virtual monochromatic dual-layer detector spectral CT imaging in unilateral and bilateral total hip prostheses. *Eur J Radiol* 2017;88:61-70
9. Große Hokamp N, Neuhaus V, Abdullayev N, Laukamp K, Lennartz S, Mpotsaris A, et al. Reduction of artifacts caused by orthopedic hardware in the spine in spectral detector CT examinations using virtual monoenergetic image reconstructions and metal-artifact-reduction algorithms. *Skeletal Radiol* 2018;47:195-201
10. Yoo HJ, Hong SH, Chung BM, Moon SJ, Choi JY, Chae HD, et al. Metal artifact reduction in virtual monoenergetic spectral dual-energy CT of patients with metallic orthopedic implants in the distal radius. *AJR Am J Roentgenol* 2018;211:1083-1091
11. Yue D, Fan Rong C, Ning C, Liang H, Ai Lian L, Ru Xin W, et al. Reduction of metal artifacts from unilateral hip arthroplasty on dual-energy CT with metal artifact reduction software. *Acta Radiol* 2018;59:853-860
12. Neuhaus V, Grosse Hokamp N, Zopfs D, Laukamp K, Lennartz S, Abdullayev N, et al. Reducing artifacts from total hip replacements in dual layer detector CT: combination of virtual monoenergetic images and orthopedic metal artifact reduction. *Eur J Radiol* 2019;111:14-20
13. Hegazy MA, Cho MH, Lee SY. A metal artifact reduction method for a dental CT based on adaptive local thresholding and prior image generation. *Biomed Eng Online* 2016;15:119
14. Wang Z, Bovik AC, Sheikh HR, Simoncelli EP. Image quality assessment: from error visibility to structural similarity. *IEEE Trans Image Process* 2004;13:600-612
15. Han SC, Chung YE, Lee YH, Park KK, Kim MJ, Kim KW. Metal artifact reduction software used with abdomi-

nopelvic dual-energy CT of patients with metal hip prostheses: assessment of image quality and clinical feasibility. *AJR Am J Roentgenol* 2014;203:788-795

16. Laukamp KR, Lennartz S, Neuhaus VF, Große Hokamp N, Rau R, Le Blanc M, et al. Correction to: CT metal artifacts in patients with total hip replacements: for artifact reduction monoenergetic reconstructions and post-processing algorithms are both efficient but not similar. *Eur Radiol* 2018;28:4524-4533

17. Kidoh M, Nakaura T, Nakamura S, Tokuyasu S, Osakabe H, Harada K, et al. Reduction of dental metallic artefacts in CT: value of a newly developed algorithm for metal artefact reduction (O-MAR). *Clin Radiol* 2014;69:e11-e16

18. Meinel FG, Bischoff B, Zhang Q, Bamberg F, Reiser MF, Johnson TR. Metal artifact reduction by dual-energy computed tomography using energetic extrapolation: a systematically optimized protocol. *Invest Radiol* 2012;47:406-414

19. Neuhaus V, Große Hokamp N, Abdullayev N, Rau R, Mpotsaris A, Maintz D, et al. Metal artifact reduction by dual-layer computed tomography using virtual monoenergetic images. *Eur J Radiol* 2017;93:143-148

고관절 인공치환술 환자에서 금속 인공물 감소 방법의 비교: 가상 단일에너지영상 대 금속 인공물 감소기법

류혜진[1,2]* · 홍성환[1,2,3] · 최자영[1,2] · 채희동[1,2]

목적 고관절 인공치환물을 가진 환자에서 여러 가지 금속인공물 감소 효과를 비교하였다.

대상과 방법 이 연구는 고관절 인공치환술과 이중에너지 전산화단층촬영을 시행한 47명 환자에서 시행하였다. 금속에서 발생한 인공물 감소효과는 서로 다른 3개의 영상(고식적 영상, 금속인공물 감소영상, 가상 단일에너지 영상)에서 비교하였다. 이를 위해 인공관절 주변 7곳에서 금속인공물에 대한 정량적 분석과 정성적 분석을 시행하였다.

결과 금속인공물 감소영상에서 가장 낮은 영상잡음과 인공물 지수를 보였고, 다음으로는 가상 단일에너지 영상이었다. 금속인공물 감소영상은 저음영 인공물이 매우 심한 영역에서만 높은 대조도를 보인 반면, 가상 단일에너지 영상은 인공물 주변 골조직과 그 외 영역에서 높은 대조도를 보였다. 연부조직 분석에서도 금속인공물 감소영상이 더 우수함을 보여 주었다. 정성적 분석에서도 금속인공물 감소영상이 가상 단일에너지 영상보다 인공물 감소 효과가 뛰어남을 밝혔지만, 이차적인 인공물 발생도 가장 흔히 발생하였다.

결론 금속인공물 감소영상이 심한 금속인공물감소에 가장 뛰어난 효과를 보였지만 새로운 이차적 인공물을 발생시켰다. 가상 단일에너지 영상은 인공물 주변 골조직 평가에서 우수함을 보였다.

[1]서울대학교병원 영상의학과,
[2]서울대학교 의과대학 영상의학교실,
[3]서울대학교 방사선연구재단